Chapter 20

Fault Stress States, Pore Pressure Distributions, and the Weakness of the San Andreas Fault

James R. Rice

Division of Applied Sciences and Department of Earth and Planetary Sciences, Harvard University, Cambridge, MA 02138, U.S.A.

Abstract

The San Andreas Fault (SAF) is weak in an *absolute* sense, in that it moves under shear stresses far smaller than implied by the most obvious reading of laboratory friction results (Byerlee law with hydrostatic pore pressure and friction coefficient $f = 0.6–0.9$). It is also weak in a *relative* sense, in that the adjoining crust seems to be mechanically stronger; this is implied by the stress state there having a horizontal maximum principal direction that makes a steep angle to the trace of the SAF, much larger than the 25–30° angle (i.e., $45° - 0.5 \arctan f$) expected from standard frictional failure considerations, and in the range of 60° to nearly 90°. It is shown that a maturely deformed fault zone which is weak relative to its surroundings, owing to inherent material strength and/or pore pressure differences, develops stresses within it which are distinct from those of its surroundings. Because of those stress differences, it is found that pore pressure distributions which are high, and near to the fault-normal compressive stress, within the fault zone, but which decrease with distance into the adjacent crust, are consistent with both the absolute and relative weakness of the SAF; the pore pressure in such distributions is less than the least principal stress at every point, so there is no hydraulic fracturing, even though the pressure in the fault zone may be greater than the least principal stress in the nearby crust. Such pore pressure distributions are shown to result from the following assumptions: (1) there is a supply of fluids near the ductile roots of crustal fault zones, where pore pressure must be nearly lithostatic; (2) active fault zones are far more permeable than the adjoining rock of the middle crust; and (3) fault permeability is a rapidly diminishing function of effective normal stress. Evidence in support of these assumptions is discussed. The resulting pore pressure distributions adjust significantly from hydrostatic, such that the effective normal stress, and hence also the brittle frictional strength, becomes approximately independent of depth along the fault zone. These assumptions also predict the possibility of diffusive surges of pore pressure that propagate upward along a fault in a slow wavelike manner.

FAULT MECHANICS AND TRANSPORT PROPERTIES OF ROCKS
ISBN 0-12-243780-2
Edited by Brian Evans and Teng-Fong Wong

Copyright © 1992 Academic Press Ltd
All rights of reproduction in any form reserved

1. Introduction

Evidence from the lack of a pronounced heat flow peak near the San Andreas Fault (SAF) show that it is weak in an *absolute* sense, in that it moves under shear stresses far smaller than the most obvious reading of laboratory friction results (Byerlee's law with hydrostatic pore pressure and friction coefficient $f = 0.6–0.9$) would seem to imply (Lachenbruch and Sass, 1980). That reading of laboratory results implies shear strength in the kilobar (10^8 Pa) range at 10 km depth, whereas the heat flow constraint suggests an average stress of order 100 bar or less over the seismogenic depth range.

More recently, results from various methods of inferring stress magnitudes and directions in the vicinity of the SAF (focal mechanism distributions, hydraulic fractures, wellbore breakouts) suggest that the fault is also weak in a *relative* sense, in that the adjoining crust seems to be mechanically stronger (Zoback et al., 1987). Relative weakness is implied since the stress state in the adjoining crust, driving the SAF, has a horizontal direction of maximum principal compressive stress σ_1 which makes a steep angle to the trace of the SAF, much larger than the 25–30° expected from the elementary frictional failure model (i.e., much larger than the angle $45° - \phi/2$, where $\phi = \arctan f$, with $f = 0.9–0.6$).

For example, Zoback et al. (1987) showed that several stress indicators suggest a maximum principal direction approaching 90° (fault-normal compression). They also note the compressional failures which take place in the nearby crust on faults striking subparallel to the SAF, and which are consistent with such a stress state; those failures accommodate the small amount of convergent plate motion which is present in addition to the primary strike-slip motion. Jones (1988) examined focal mechanisms of earthquakes on known faults within 10 km of the SAF and inferred that these, if regarded as being driven by a uniform stress field, required maximum stress directions in the range of 60–70° to the SAF, for the four of five regions studied in which the resulting σ_1 was horizontal. Similarly, along the strand of the Calaveras Fault active in the 1984 Morgan Hill earthquake, Oppenheimer et al. (1988) inferred a σ_1 direction in the adjoining crust of 60–80° at the time of the earthquake, for consistency of focal mechanisms of the aftershock sequence with the sum of that initial stress state plus the stress change associated with faulting. Such steep angles mean that the adjoining crust supports substantially more shear stress than does the SAF (or the Calaveras Fault).

It is likely that many major intraplate and interplate zones of active faulting are similarly weak. Fault weakness in continental thrust sheet emplacement is well known (Hubbert and Rubey, 1959), and recent works have emphasized the weakness, in both relative and absolute sense, of decollement faults beneath sediment-dominate accretionary prisms (Byrne and Fischer, 1990) and of transform faults along the ocean floor (Wilcock et al., 1990).

There seems to be no alternative to assuming that local stresses compatible with laboratory-measured friction properties are present in fault zones where seismic ruptures nucleate. Laboratory results suggest that classical friction concepts with f in the range 0.6–0.9 (Byerlee, 1978) describe the onset of sliding in most crustal rocks. Also, values of f in that range are known to be consistent with stress states on natural faults as inferred at approximately 2 km depth in the Rangely oilfield experiment (Raleigh et al., 1976), on faults intersected along the 3 km depth of the Cajon Pass borehole (Zoback and Healy, 1991), and generally on faults as studied at shallow depths by borehole stress measurement (e.g., Zoback et al., 1980; Hickman, 1991).

Explanations of fault weakness may thus be based on the assumption of presence at seismogenic depth of frictionally weak fault zone materials, like water-absorbing

seismogenic depth of frictionally weak fault zone materials, like water-absorbing montmorillonite clays, although dewatering to illite and related frictional strengthening of such materials is likely to set in at temperatures above about 200°C (see, for example, Morrow et al., this volume, Chapter 3). They may also be based, more speculatively, on severe stress concentrations along the edges of isolated locked patches in a fault zone, owing to some mechanism of slow creep at low stress in neighboring fault zone material, provided that those locked patches slip-weaken very rapidly after instability begins (so that average stresses are small and stress drops, as conventionally inferred, appear to be far smaller than the actual kilobar range that would then be implied at the rupture-nucleating stress concentration site, if $f = 0.6–0.9$ and p is hydrostatic). Yet another possibility is that they may be based on elevated pore pressures in a fault zone having the usual frictional properties, $f = 0.6–0.9$. While it is possible that some combination of these explanations, and maybe others not yet elaborated, are sources of fault weakness, the aim here is to evaluate the pore pressure explanation.

It is shown that pore pressure distributions which are high and near to the normal stress within a major fault zone, but lower in the adjacent crust, are consistent with both the absolute and relative fault weakness discussed. Further, it is shown that such pore pressure distributions result from assumptions about crustal fluids and their motion which have extensive support from geochemical, petrologic and geophysical observations.

Since the work of Hubbert and Rubey (1959), high pore pressure has been appreciated widely as a plausible cause of what, here, has been called absolute fault weakness. Nevertheless, the more recent understanding of the *relative* weakness of major faults, signaled by the steep angle of σ_1, has led many to the conclusion that some explanation other than elevated pore pressure is required. This is because the pore pressure needed had seemed to be larger than the least principal stress. It is shown in the next section that such a conclusion is based on the tacit assumption that the stress tensor within the core of a mature fault zone like the SAF is fully identical to that in the nearby crust at the same depth. Instead, an analysis of the mechanics of a maturely deformed fault zone shows that these stress tensors differ in an essential way, with consequence that the pore pressure distributions required for relative fault weakness can meet, at every point, the condition that pore pressure be less than the least principal stress at that point, even though the pore pressure within the active fault core may be larger than the least principal stress prevailing a short distance away in the adjacent crust. (Independently, Byrne and Fisher (1990) have made similar mechanical arguments for a weak and overpressurized decollement beneath a sediment-dominated accretionary prism, and they also noted in their closing discussion the relevance of the concept of the SAF. Also, Byerlee (1990), in a study first presented at the same conference as was the present work, but published elsewhere and hence earlier, considers a clay fault gouge that is assumed to seal permanently a gradient of pore pressure perpendicular to itself. He comes to similar conclusions regarding stress states within and outside the fault core for the special case of fault-normal compression. In a recent work, Fournier (1990) addresses the fault weakness problem by assuming that fault zones, sealed by mineralization, can accommodate pore pressures significantly in excess of the least principal stress.)

2. Fault Stress States and Effects of Variations of Strength or Pore Pressure

It is shown here that the mechanics of a maturely deformed fault zone, which is weak relative to its surroundings owing to inherent material strength and/or pore pressure

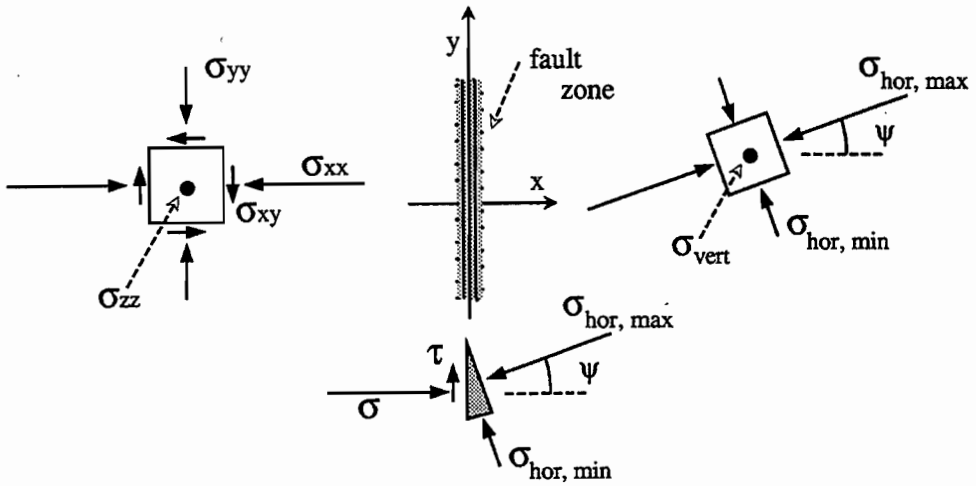

Figure 1. Stress state as seen in a horizontal plane through a vertical strike-slip fault zone. Axis y is horizontal and along the fault trace, x is perpendicular to the fault, and z is vertical.

differences, is such that a different stress state develops within the fault zone than in its surroundings. This result is applied to a fault zone such as the SAF and its adjacent crust, in the case for which both regions are assumed to have identical mechanical properties, including laboratory-like friction properties, but to sustain nonuniform pore pressure. It is found that pore pressure distributions which are high and near to the fault-normal compressive stress within the fault zone, but which decrease with distance into the adjacent crust, are consistent with both the absolute and relative weakness of the SAF. For example, stress distributions may exist for which a vertical fault such as the SAF is at a critical state for *strike-slip* failure, while the adjacent crust is at a critical state for *thrust* failure under a principal direction making an angle to the SAF that becomes *arbitrarily large* (but less than 90°) as pore pressure within the fault zone approaches the fault-normal compression there.

It is straightforward to see why high pore pressure has seemed incompatible with the steep σ_1 angle when such stress state differences are neglected. Figure 1 corresponds to a plane parallel to the earth's surface along a strike-slip zone like the SAF. The y-axis points along the fault trace in that plane and the x-axis is perpendicular to it; z is vertical. The direction of the maximum horizontal stress $\sigma_{\text{hor,max}}$ is assumed to make an angle ψ with the normal to the fault (this angle notation is used throughout, so that a steep $\sigma_{\text{hor,max}}$ direction corresponds to a small value of ψ, the $\sigma_{\text{hor,max}}$ direction being at angle $90° - \psi$ with the fault trace). The minimum horizontal stress is denoted $\sigma_{\text{hor,min}}$. Cartesian stress components are also shown in Figure 1. If the stress state is to be understood as being critical for thrust failure in the nearby crust, as happens near the SAF, so that σ_1 is horizontal and σ_3 vertical, then $\sigma_{\text{hor,max}} = \sigma_1$ and $\sigma_{\text{hor,min}} = \sigma_2$.

The normal stress σ and shear stress τ acting along the fault (Figure 1) are

$$\sigma = \tfrac{1}{2}(\sigma_{\text{hor,max}} + \sigma_{\text{hor,min}}) + \tfrac{1}{2}(\sigma_{\text{hor,max}} - \sigma_{\text{hor,min}}) \cos 2\psi$$

$$\tau = \tfrac{1}{2}(\sigma_{\text{hor,max}} - \sigma_{\text{hor,min}}) \sin 2\psi$$

We assume that for slip along the fault, the friction condition

$$\tau = f(\sigma - p) = \tan \phi(\sigma - p)$$

must be met, where p is the local pore pressure and $f = 0.6$–0.9 (so that $\phi = 31$–$42°$). Solving for the value of p which just suffices to meet the friction condition then gives

$$p = \sigma_{\text{hor,min}} - (\sigma_{\text{hor,max}} - \sigma_{\text{hor,min}}) \cos\psi \sin(\psi - \phi)/\sin\phi$$

This equation shows that the required p will exceed $\sigma_{\text{hor,min}}$ whenever the maximum stress is at a sufficiently steep angle to the fault that the angle ψ of Figure 1 is less than ϕ (this observation has been made by Sibson, 1985). Further, if $\sigma_{\text{hor,min}}$ is σ_2, then p will exceed the vertical stress σ_3 under an even less stringent condition. This means that p will exceed $\sigma_{\text{hor,min}}$ whenever ψ is less than an angle of 30–40°, or whenever the angle $90° - \psi$, which $\sigma_{\text{hor,max}}$ makes with the fault direction, is greater than 50–60°. The steep angles mentioned above fall in the range of 60° to nearly 90°, and thus call for $p > \sigma_{\text{hor,min}}$. On this basis, it had been assumed that the steep angles could not be explained in terms of fault weakening by high pore pressure, since such pore pressures would lead to hydraulic fracture.

However, the argument just gone over is not strictly correct, at least if we regard the stress state with values $\sigma_{\text{hor,min}}$ and $\sigma_{\text{hor,max}}$, at angle ψ, as referring to the stress state in the nearby crust adjacent to a maturely deformed fault zone. This is because the stress state within a heavily deformed fault zone that is weakened either by having locally high pore pressure or by being made of inherently weak material will not be the same as the stress state in the nearby crust. Rather, there will develop larger principal stress magnitudes within the fault core than in the nearby crust, as shown below, when there is a small angle ψ in the nearby crust. Thus, even though one must expect the pore pressure to be higher within the fault core than in the nearby crust (as shown in the next two sections to follow from reasonable assumptions on the presence and motion of fluids in the crust), it develops that the pore pressure in the fault core is still less than the (locally elevated) least principal stress in the core, so that hydraulic fracture is not a problem. This is so even though the locally high pore pressure in the fault core is greater than the least principal stress prevailing at other locations, some distance away in the nearby crust.

If the stress state does vary near a fault zone, it is reasonable to think of the stresses at a given depth (in the vicinity of the fault zone and at locations not too near the earth's surface) as effectively varying only with the coordinate x, where x is measured perpendicular to the fault zone. For the strike-slip case in Figure 1, x is horizontal. Then, if we let the y-direction be along strike, and z vertical, it will be evident from conditions of mechanical equilibrium that the stress components σ_{xx} $(= \sigma)$, σ_{xy} $(= \tau)$, and σ_{xz} (assumed to vanish in the discussion above) must be essentially the same everywhere within the deforming fault zone as in the nearby crust outside it. There is no reason, based on equilibrium considerations, that σ_{yy}, σ_{zz}, and σ_{yz} (the latter also assumed above to vanish) should be essentially the same within the fault zone as outside it. Rather, the appropriate values of σ_{yy}, σ_{zz}, σ_{yz} are determined from mechanical constitutive relations, so as to assure that the material within the fault zone, deforming primarily if not exclusively by strike-slip shear, has essentially the same components of strain rate ε_{yy}, ε_{zz}, and ε_{yz} at points within the fault as outside. These are the components of strain rate governing distortions of planes lying parallel to the strike-slip fault plane. Just as the equilibrium conditions on the problem restrict σ_{xx}, σ_{xy}, and σ_{xz} to continuity, but leave σ_{yy}, σ_{zz}, and σ_{yz} unrestricted, so do the kinematical conditions on the problem restrict the strain rates ε_{yy}, ε_{zz}, and ε_{yz} to continuity but leave ε_{xx}, ε_{xy}, and ε_{xz} unrestricted;

here 'continuity' is to be interpreted as meaning having no strong variations as one passes along the x direction in the vicinity of the fault.

As is best illustrated by the simple example which follows, these considerations will require that if a maturely deformed fault zone is weak either because it is made of inherently weak material, or because of a pore pressure distribution which involves higher pressure within the fault zone than in the adjacent crust, then the equations of continuum mechanics generally preclude the possibility that all components of stress are the same within and outside the zone. In particular, the stress components σ_{yy} and σ_{zz}, for which variation with x is not constrained by equilibrium considerations, will be seen to vary significantly as we traverse the fault zone in the x-direction.

2.1. Simple example, soft ductile layer in hard ductile surroundings

A simple example is useful to clarify the significance of these remarks. It is done not for the case of primary interest here, involving a frictional material with sensitivity to pore pressure, but rather for the simpler case of classical rigid–plastic solids, for which the result will, hopefully, be found somewhat intuitive. Figure 2 shows a thin, soft ductile layer that is embedded within a harder ductile solid. Here, by 'ductile' is to be understood that the materials undergo volume-preserving plastic flow ($\varepsilon_{yy} = 0$) which is dependent, in the von Mises manner, on only the deviatoric stress components $s_{\alpha\beta}\,(= \sigma_{\alpha\beta} - \frac{1}{3}\delta_{\alpha\beta}\sigma_{\gamma\gamma})$

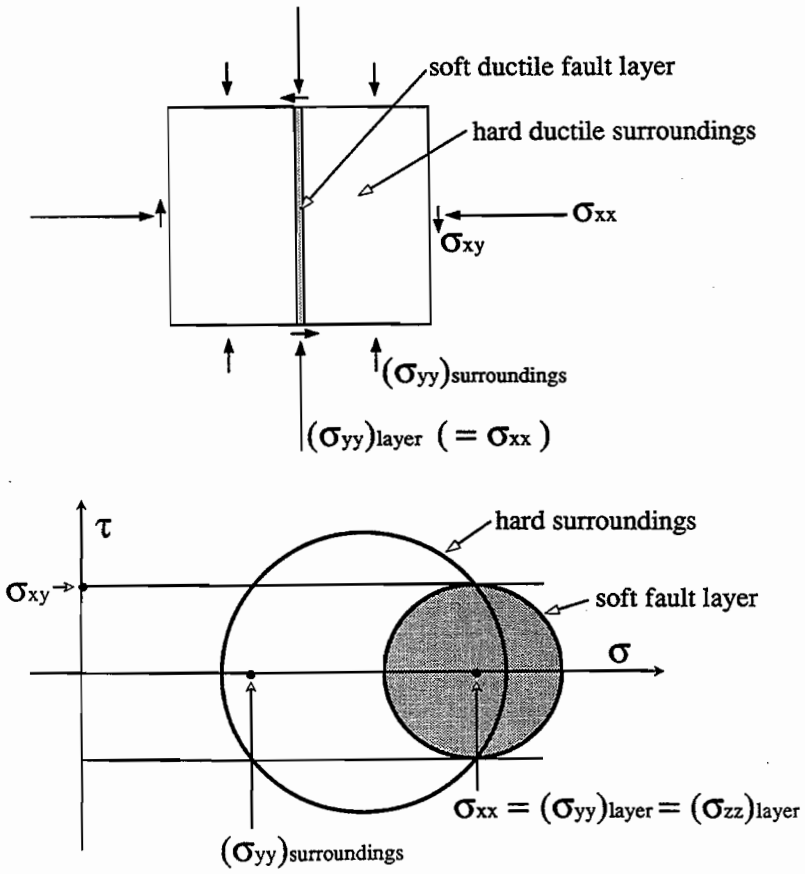

Figure 2. Stress states associated with the deformation of a soft ductile layer in harder ductile surroundings. The stress field induced in the layer is different from that in the surroundings.

and not on the mean normal stress ($\frac{1}{3}\sigma_{\gamma\gamma}$); here $\alpha, \beta, \gamma = x, y, z$, with the usual summation convention on repeated indices. Further, the strain rates partition themselves among components so that the ratio of any $\varepsilon_{\alpha\beta}$ to $\varepsilon_{\gamma\delta}$ is the same as the ratio of $s_{\alpha\beta}$ to $s_{\gamma\delta}$.

The system is stressed with a large compression σ_{xx} acting perpendicular to the fault layer, but still of a magnitude well short of that to cause plastic flow in the harder solid, and with a shear stress σ_{xy} which suffices to cause the soft layer to flow plastically. Since the harder solid is nondeforming, all strain rates vanish within it and, since strain rate components ε_{yy}, ε_{zz}, and ε_{yz} must be the same within the fault layer as outside it, those same components vanish also within the layer. By incompressibility, $\varepsilon_{xx} = -(\varepsilon_{yy} + \varepsilon_{zz}) = 0$ additionally within the layer. Thus the soft fault layer can deform only in simple shear relative to its boundaries, and from the symmetry of the situation, ε_{xy} is the only nonzero strain rate within the layer. The constitutive relations thus require that all deviatoric stress components except s_{xy} ($= \sigma_{xy}$) vanish within the layer, and, in particular, this means that $\sigma_{yy} = \sigma_{zz} = \sigma_{xx}$ within the layer, where (from the required continuity of the set of stresses σ_{xx}, σ_{xy}, and σ_{xz}) the σ_{xx} here is the same within the layer as that applied to the harder solid outside it.

Thus the stress components σ_{yy} and σ_{zz} within the soft fault layer bear no relation whatever, in this example, to those stress components of the same subscripts which act on the harder solid at points remote from the fault zone. Mohr circles for the soft fault layer and for the adjoining hard solid are shown in Figure 2. Continuity of σ_{xx} ($= \sigma$) and σ_{xy} ($= \tau$) requires that both circles share this common (σ, τ) point of the Mohr plane. Although the soft layer sustains much less shear stress (smaller-diameter circle) than the harder surroundings, the principal stresses that develop within the soft layer, of which horizontal components are given by the σ-axis intercepts, are significantly larger than those for the stronger surroundings.

A few comments are in order before moving on from this simple example. First, reference was made in the introductory remarks to stress states being dissimilar between a 'maturely deformed' fault zone and its surroundings. A mature deformation state has been tacitly assumed in this example by adoption of a rigid-plastic model and solution for a more or less steady deformation rate field. If, instead, we imagined the system to be initially stress-free and then loaded it with σ_{xx} and σ_{xy} as discussed, the stresses σ_{yy} and σ_{zz} within the fault layer would not initially coincide with σ_{xx}, but rather would approach that value with ongoing plastic deformation; an elastic–plastic, rather than rigid-plastic, model would be needed to model such a transition.

Second, the case discussed thus far assumed that the harder solid did not deform. This is not such a good analog of the crust near the SAF, which accommodates some convergent deformation. We might therefore consider the case for which the stress state applied to the harder surroundings suffices to cause it to flow plastically, in a mode that must, in general, be expected to involve nonzero ε_{zz}, and perhaps ε_{yy}, as well as nonzero ε_{xx} (the convergent component) and ε_{xy} (nonzero since a finite σ_{xy} is sustained). The same strain rates ε_{zz} and ε_{yy} must be sustained within the soft layer, which, in addition, can be made (by application of suitable σ_{xy}) to take on any ε_{xy} value, not constrained kinematically by that outside. In the general case, all the $\varepsilon_{\alpha\beta}$ within the soft layer could be of comparable order, and there would be no need for, say, σ_{yy} within it to be close in value to σ_{xx}. However, to pursue our SAF analogy, the fault zone must be relatively thin compared to dimensions of the deforming hard block outside it, and the net convergent displacement accommodated is modest compared to the strike-slip motion. In such cases ε_{xy} within the soft fault layer must be much greater than any $\varepsilon_{\alpha\beta}$

in the harder solid outside, and in this case all $s_{\alpha\beta}$ except σ_{xy} within the soft layer will be small compared to σ_{xy}. Thus, for all practical purposes we recover the result $\sigma_{yy} = \sigma_{zz} = \sigma_{xx}$ within the layer, just as above for the case of a nondeforming outer region.

Third, there is no need to confine attention to a single soft layer. Instead one could consider an array of thin layers joined together, the array being still thin in aggregate, and embedded in a stronger outer solid. In the limit, this would represent a continuous variation of plastic strength, for example, weakest in the center of the fault zone and increasing as one moves away in the $+x$ or $-x$ directions. The principles of analysis are the same as above, with stress components σ_{xx}, σ_{xy}, σ_{xz}, and strain rate components ε_{yy}, ε_{zz}, ε_{yz}, being independent of x in the vicinity of the fault zone, and with the constitutive law obeyed everywhere. The details are somewhat complex, but it is easy to see that the nonconstrained stress and strain rate components will vary continuously with x, over the same portion of the x-axis as that over which the plastic strength varies. Also, the ratio of local strike-slip ($2\varepsilon_{xy}$) to convergent (ε_{xx}) deformation is position-dependent, and is largest at the weakest plane within the fault zone, where, if conditions as at the end of the previous paragraph apply, one will again have, approximately, $\sigma_{yy} = \sigma_{zz} = \sigma_{xx}$.

Finally, this analysis has been simplified by assuming a narrow fault region near which components of $\sigma_{\alpha\beta}$ and $\varepsilon_{\alpha\beta}$, if they vary at all, are assumed to vary only with distance x perpendicular to the fault. That is, $\partial/\partial x$ has been assumed to be of larger order than $\partial/\partial y$ or $\partial/\partial z$. Such will not generally be an acceptable approximation at shallow locations along the fault, at depths within a few fault zone widths of the free surface.

2.2. Brittle fault zone, variable pore pressure

Figure 3 shows stress states at a location within a brittle fault zone, presumed to represent the SAF, and in the adjacent, also brittle, crust. Pore pressure is imagined to be somewhat higher within the fault zone than outside, for reasons discussed in a subsequent section. The pore pressure varies continuously with x, from the maximum at, say, $x = 0$ in the fault core to a smaller value in the nearby crust at the same depth. In contrast to the simple example above, we assume here that the fault zone and the adjacent crust have identical strength properties, i.e., that both regions share the same friction coefficient f and obey the same law that 'failure' occurs when, and on the plane for which, the Amonton–Coulomb inequality $\tau < f(\sigma - p)$ is first violated. We assume that f is of the order of what is suggested by laboratory results, e.g., in the range from about 0.6 to 0.9. Hence, in this example, any difference in the stress and deformation response is rooted in the assumed variation in pore pressure. Figure 3 also emphasizes that not all stress components are required to be the same within the fault zone and in the adjacent crust.

Figure 4 has been prepared on the understanding, motivated by the previous subsection, that the local stress states within and near the brittle fault zone will adjust themselves to be compatible with the local deformation condition. The overall displacements accommodated are assumed to involve strike-slip along with some modest fault-normal convergence. This figure depicts coexisting stress states within the central core of a strike-slip fault at the most pressurized location, $x = 0$, and in the adjacent crust. The Mohr circles referring to horizontal stresses are shown as solid lines, and these intersect at the common point (σ, τ) of the Mohr plane, corresponding to the

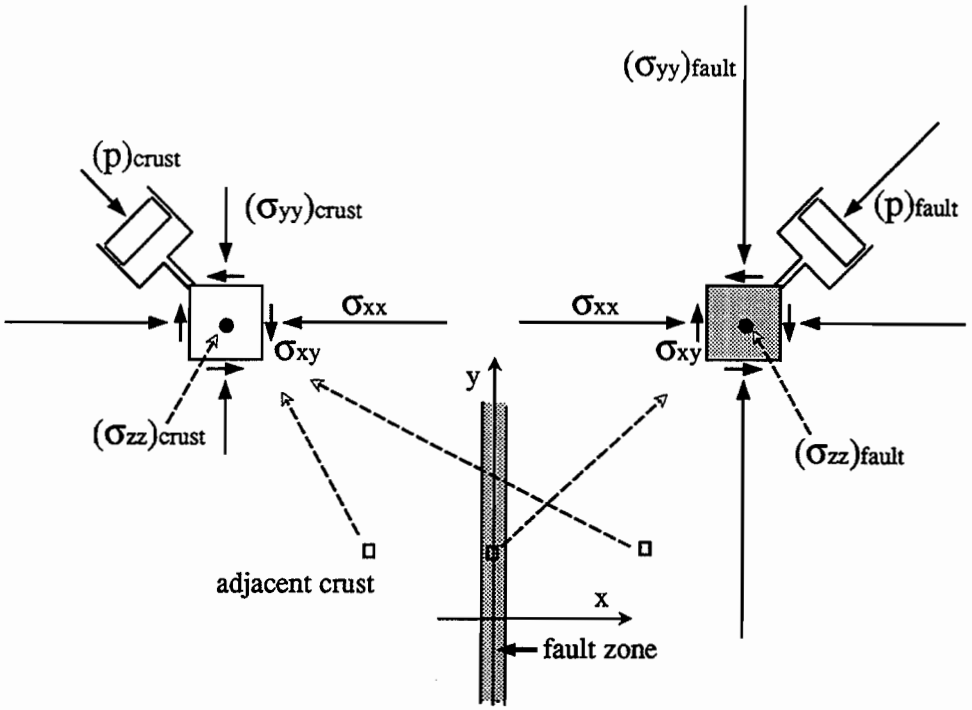

Figure 3. Stresses and pore pressure at locations within the core of the fault zone and in the adjacent crust. It is assumed that the pore pressure is high within the fault zone and diminishes somewhat with distance into the adjacent crust.

values of the fault-normal compressive stress σ_{xx} $(=\sigma)$ and fault-parallel shear stress σ_{xy} $(=\tau)$ depicted in Figure 3. Mohr circles involving vertical stress are shown as dashed lines in Figure 4. The largest Mohr circles in both regions meet the same Amonton–Coulomb failure condition, that $\tau = f(\sigma - p)$, where here τ and σ refer to the local stress values where the relevant Mohr circle has tangential contact with the limiting stress line, as illustrated. This happens on the plane $x = 0$ for the strike-slip failure within the fault core, and on a dipping thrust fault in the adjacent crust, trending subparallel to the SAF.

For the case illustrated, with friction coefficient $f = 0.7$ $(\phi = 35°)$, the fault zone core is critically stressed for strike-slip failure, and the principal stress direction within it makes the (proper) shallow angle of 27.5° $(= 45° - \phi/2)$ to the fault while, simultaneously, the adjacent crust is critically stressed for thrust failure under a steep principal direction at 72° $(= 90° - \psi$, where $\psi = 18°$ here) with the strike-slip fault. As will be evident from the construction, greater pore pressure within the fault, becoming closer to σ_{xx} (i.e., to the ordinate at which the two solid-line Mohr circles intersect), or closer to the local least principal stress in the fault core, would allow ψ to be as small as one would like.

Thus strike-slip failure, under conditions approaching fault-normal compression, is perfectly compatible with laboratory-range rock friction properties, so long as a mechanism exists for there being high pore pressures within the fault that grade to lower pressures in the immediately adjacent crust.

A range of values for the vertical stress within the fault core is possible in the construction of Figure 4, so long as that stress does not lie outside the range of the horizontal principal stresses there. If the fault core were to simultaneously meet conditions

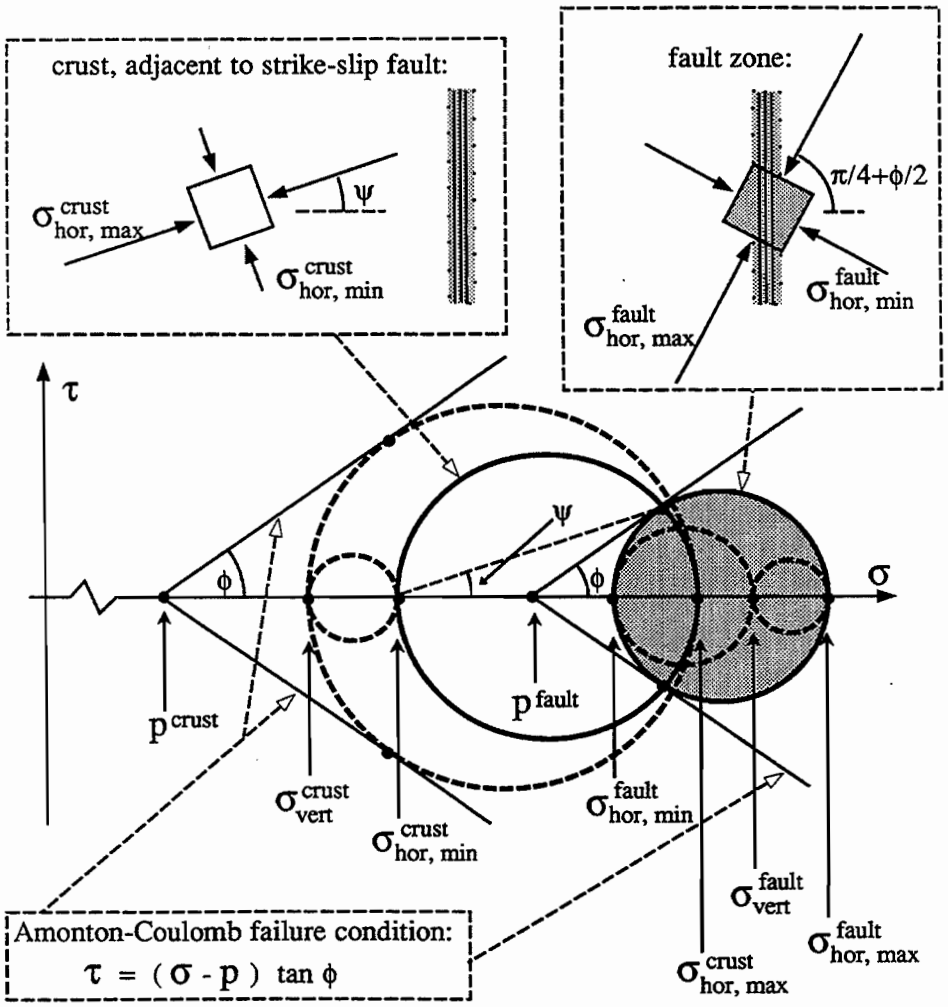

Figure 4. Example of failure under a stress state with maximum principal direction at a steep angle to a strike-slip fault. Construction shows stresses which are critical for strike-slip failure within the fault core and for thrust failure in the adjacent crust. Pore pressure and stresses are assumed to vary continuously, with distance x, between those of the two states shown. At each point the pore pressure is less than the least principal stress, although the pore pressure within the fault core is greater than the least principal stress in the adjacent crust. Drawn for $\phi = 35°$ ($\tan\phi = 0.7$) and $\psi = 18°$.

of strike-slip and thrust failure, as discussed in connection with the ductile layer example, then the vertical stress within the core would coincide with the least horizontal stress there. Unfortunately, the brittle case cannot be analyzed in the same precision as for the simple ductile layer, since failure involves stress drops rather than simple plastic flow at fixed stress, and, further, even in circumstances of stable frictional deformation, there is no generally agreed description of the combined stress state dependence of the flow process, analogous to the von Mises type formulation used for the ductile layer.

For such stress and pore pressure distributions as contemplated in connection with Figures 3 and 4, the pore pressure p is less than the least principal stress σ_3 at every point of the region, so there need be no hydraulic fracturing, even though p in the fault zone core may, in conditions like those illustrated, be greater than σ_3 at some distance away in the adjacent crust. Both p and σ_3 diminish with distance from the fault core,

transitioning to values appropriate to the adjacent crust where σ_3 equals the overburden. At points near the fault core in that transition region, shear deformation of type γ_{xy}, less intense than in the core itself, is expected to induce some local elevation of σ_{yy} and σ_{zz} (and hence of σ_3), by the mechanism discussed above, so that $p < \sigma_3$ is met throughout the region of elevated p. These concepts seem to remove the difficulty some have had, based on the reluctance to accept fracture-inducing pressure levels, in reconciling the relative weakness of the SAF with elevated pore pressures. (Still, elevated pore pressures do sometimes lead to hydraulic cracking in seismogenic fault zones (Kerrich, 1986; Sibson, 1990), and the mechanism by which fluid transport is maintained in the crust, against depositional pore sealing processes, may involve pervasive hydraulic fracturing (Fyfe et al., 1978)).

We may conclude at this point that pore pressures which become close to the fault-normal compressive stress in the fault core, and which are somewhat lower in the adjacent crust, are consistent with both the absolute and relative weakness of major faults such as the SAF. Further, this is so even when the fault zone and nearby crust have identical strength properties, comparable to those found for rocks in the laboratory. The next two sections explain why it may be reasonable to expect such pore pressure distributions actually to be present in the crust.

3. Crustal Plumbing and Origin of Fault Zone Pore Pressure

Some assumptions about the supply of fluids in the crust and about the relative permeability of transport paths are stated below. All have substantial observational support. Fluid transport in the crust is complicated by a competition between depositional processes which seal-off permeability (e.g., Smith and Evans, 1984) and rupture processes which renew pore connectivity; the latter involve seismic and sometimes aseismic shear failures and, often, local tensile cracking driven by pressure build-up along clogged flow paths (Fyfe et al., 1978; Kerrich, 1986; Nur and Walder, 1990; this volume, Chapter 19; Sibson, 1990). It is thus a great simplification to treat the pore pressure distribution in the crust as resulting from solutions to the steady, time-independent equations for flow in porous media, as will be done here.

Nevertheless, within that simplification, relatively straightforward analysis (given in the next section) shows that if the assumptions to be stated hold good, then under a fairly wide variety of conditions there results a pore pressure distribution with the following characteristics: p is moderately close to the normal stress σ over nearly the entire fault depth, excepting a regime near the earth's surface where pressure variation with depth can be closer to hydrostatic, and p at sites only a few kilometers away from the fault zone, in the adjoining crust at seismogenic depths, is considerably lower. That is, of course, the type of pore pressure distribution which has been shown above to imply both absolute and relative fault weakness.

The assumptions are:

1. There is a source providing fluids deep in the crust near the ductile root of the fault zone, and pore pressures there approach lithostatic values (the second part of this assumption may be argued to follow from the first, since pore pressure within a source region in ductile rock must necessarily be near to lithostatic; otherwise, pore spaces would creep shut).

2. The core of a tectonically active fault zone, where pore connectivity is renewed by shearing, is much more permeable than the adjoining rock of the middle crust. (Another version of this assumption, sufficing either separately or in combination with that stated, is that the active core is much more permeable in directions along the plane of the core than perpendicular to it.)
3. Permeability along the fault zone is a strongly decreasing function of the effective normal stress, and hence is a strongly increasing function of pore pressure.

Because complete data are not always available from along the SAF, and because the phenomenon of weakness of major, crust-cutting faults is thought to be more general, observational data pertaining to these assumptions from many fault zones are reviewed here (in sequence 2, 1, 3).

3.1. Assumption 2

The assumption that fault zones are the preferred fluid permeation routes seems to be widely accepted on the basis of petrologic studies of exhumed fault zones. Such studies, involving compositional alterations along faults and fluid inclusions, are generally interpreted to show that large amounts of fluid (H_2O, CO_2) have moved through fault zones (Sibson et al., 1975; Beach, 1980; Newton et al., 1980; Etheridge et al., 1984; Kerrich, 1986; Parry and Bruhn, 1986; McCaig, 1988).

Geochemical tracers along *currently active* faults provide another basis for assumption 2. An elevated $^3He/^4He$ ratio for helium within crustal fluids is thought to be a definitive indicator of a mantle origin for that helium. In a general survey of helium in groundwater outflows in Western Europe, Oxburgh and O'Nions (1987) and O'Nions et al. (1989) show coincidence between areas where helium of mantle origin emerges and areas of currently active tectonics (mostly by extensional faulting in the area studied). This suggests that active fault zones are much better conduits for deep fluids than are stable areas of the crust and older, now inactive, fault zones, where groundwater emanations are not found to have elevated $^3He/^4He$ ratios. The helium is generally thought to occur in association with mantle-derived magmas emplaced into the middle or shallow crust, and this is thought to be most common in extensional tectonic regimes. Nagao et al. (1990) have recently given a preliminary report on the release of mantle-derived helium, and of CO_2 compatible with a mantle origin, in the strike-slip environment along the North Anatolian Fault in Turkey. Helium outflows of mantle origin, correlated with locations of active faulting, have been reported (Wakita et al., 1987) in a nonvolcanic forearc area of crustal seismicity in the Kinki District, Japan, and in association with the fault of the 1966 Matsushiro swarm (Wakita et al., 1978).

No general survey of helium emanations in groundwater outflows along and adjacent to the SAF has yet been reported. There are data on the Salton Trough area (Whelan et al., 1988; H. Craig, private communication, 1990) and the general occurrence of areas of elevated $^3He/^4He$ seems better explained in terms of shallow magmatic activity than fault location. There are, however, locations with elevated $^3He/^4He$ along the SAF, and such emanations as reported in the East Mesa area do not have an obvious shallow magma source. Irwin and Barnes (1980) point out that the areas of North America with greatest CO_2 discharge in spring outflow include the Franciscan rocks of the coastal ranges near the San Andreas fault. They reported that the $\delta^{13}C$ values along the SAF are compatible with a mantle origin, although carbon isotopes do not provide an unambiguous tag of origin. Thus, while the depth of origin of the CO_2 is not certain,

its outflow in carbonic springs does support the notion of the fault as an effective transporter of fluids. While abundant, such springs certainly do not occur everywhere along the SAF. A speculation (R. Fournier, private communication, 1990) is that upwelling of CO_2 may be rather pervasive, but that clay gouge in the shallow reaches of the fault provides a seal so that massive leakages sufficient to feed carbonic springs are relatively rare events along-strike.

An additional insight on assumption 2 is provided by seismic inferences of fault zone properties. These have been carried out extensively for the New Madrid zone. Al-Shukri and Mitchell (1988) show that the *p*-wave velocity is reduced near the fault, and that inferred contours of lower velocity coincide well with the seismically most active part of the zone (and not, for example, with older, now inactive regions). This is shown in *p*-wave contours for both the 0–5 km and the 5–14 km depth ranges, spanning the depth of current seismicity there. Al-Shukri and Mitchell (1990) and Hamilton and Mooney (1990) show similar correlations with seismic attenuation. In studies of the response to blasts along refraction lines, the latter show that very weak arriving signals result for ray paths that traverse the currently active area, compared to the strength of signals for paths that avoid the fault or traverse now-inactive fault areas. While the interpretation of such results is not unambiguous, they strongly suggest that the currently active part of the fault is a region of increased porosity and crack content compared to the nearby crust, and hence would be fluid-infiltrated. The lack of such velocity and attenuation anomalies from now-inactive fault zones suggests that these have had their porosity filled in by depositional processes; this may be expected, as they now lack the essential effects of (shear) fracturing on renewal of pore connectivity and maintenance of permeability.

For the San Andreas system, Mooney and Ginzburg (1986) review evidence from seismic reflection studies, gravity (see also Wang et al., 1986), and other sources to conclude that the fault zone is a zone of reduced wave speeds and reduced density. They suggest that the zone of altered properties extends up to 3–4 km width along the creeping portion of the SAF to as little as 0.2 km or less along locked portions that fail in large earthquakes. Mooney and Ginzburg (1986) likewise suggest an interpretation of that zone of altered properties as one of increased porosity and fluid infiltration.

The interpretation to be made of assumption 2 is that the ratio $k_{\text{crust}}/k_{\text{fault}}$ is very much less than unity, where k_{crust} is the permeability of the middle crust outside the seismogenic fault zone, and k_{fault} the permeability within the fault zone. The smallness of the ratio is what controls the character of the predicted pore pressure distribution. Thus, for a ratio of 10^{-3}, it will not matter if $k_{\text{fault}} = 1$ μd (d = Darcy = 10^{-12} m^2) and $k_{\text{crust}} = 1$ nd, or if $k_{\text{fault}} = 1$ md and $k_{\text{crust}} = 1$ μd (except that, judging from the results of Peacock (1990), fluid permeation would have negligible effect on the crustal temperature distribution in the former case but would perturb it somewhat, depending on the thickness of the permeable part of the fault zone, in the latter).

An alternate version was given for assumption 2 that has experimental support in that Arch and Maltman (1990) show, for sediments deformed in a laboratory shear apparatus, the development of distinctly anisotropic permeability that is several times larger in the direction perpendicular to the shear zone than along it. The amount of shear is small compared to that of a maturely deformed fault zone, in which the effect may be much larger. This alternate form of assumption 2 is also encouraged by the viewpoint that the core of a mature fault zone contains finely pulverised rock and sometimes appreciable clay components. These are not very permeable materials, and

may form a very low-permeability lining to the walls of the highly deforming central portion of the fault zone. (In fact, Byerlee (1990) regards the entire width of the SAF fault zone as completely impermeable, in all directions, for pressure gradients below a critical threshold; this may be too extreme.) Thus there could be transport along the rupturing fault core, for reasons already discussed in connection with assumption 2 here, but little transport perpendicularly across the fault zone; this is equivalent at a more macroscopic scale to anisotropic permeability in the fault zone. It is again the smallness of a permeability ratio, now k_x/k_z, which matters in the assumption, rather than absolute values, where subscripts x and z denote permeability within the fault zone in directions respectively perpendicular and parallel to the plane of the fault core.

3.2. Assumption 1

The assumption on fluid presence near the ductile roots of fault zones has strongest evidence from magnetotelluric investigations. In these, the lower crust frequently shows a far smaller electrical resistivity than could be expected for dry rocks (Shankland and Ander, 1983; Haak and Hutton, 1986; Hyndman and Shearer, 1989; Madden et al., 1990). Further, areas that are tectonically active at present generally show the lowest values, typically less than 100 Ω m, assuming a 10 km conductive layer. Hyndman and Shearer (1989), following Shankland and Ander (1983), argue that the conductivity strongly suggests the presence of water in interconnected pore spaces in the lower crust. In view of the elevated temperatures there, the pore spaces are argued to have the form of quasiequilibrium tubular networks along grain triple junctions. Hyndman and Shearer (1989) infer that if the water is of salinity roughly like seawater, as fluid inclusion studies and the temperature dependence of resistivity (Shankland and Ander, 1983) suggest, that a porosity from about 0.5% to 3% is necessary in the lower crust for consistency with the low electrical resistivity.

Following earlier work correlating the inferred depth to the upper lid of the conductive layer with heat flow, Hyndman and Shearer (1989) note that the lid is in the temperature range of about 350–400°C, which reasonably coincides with temperatures at the lower limit of the seismogenic depth range as discussed in recent years by Brace and Kohlstedt (1980), Chen and Molnar, 1983), Sibson (1982) and Meissner and Strehlau (1982).

Thus the resistivity results imply that fluids are present at the ductile roots of major fault zones that traverse the crust, as in assumption 1. As mentioned there, the pore pressure in fluids long residing within ductile rocks must be lithostatic (or a modest amount above, to balance the forces stemming from surface energy that would otherwise cause sintering). Very interesting questions are raised by the presumed presence of fluids in the lower crust. Their exploration would take us too far afield here (see Gough, 1986; Hyndman and Shearer, 1989; Bailey, 1990), but they include the mechanisms of long-time sealing at the upper lid of the conductive layer, at least at positions away from its intersection by an active fault core, the reasons for the approximate coincidence found between the depth to the lid with that to the onset of lower crustal reflectors, which are usually also numerous in tectonically active areas, and the relation of both of those features to mid-crustal decollements.

Among possible sources for fluids near the ductile roots of fault zones is the release of volatiles, primordial or recycled, from the mantle or from underthrust crustal terrains. Newton (1989, 1990), O'Nions and Oxburgh (1988), and Sheppard (1989) provide recent reviews of the evidence on this. (Gold and Soter (1985) present a strong advocacy of the control of earthquake phenomena by deep fluid sources.) The use of $^3He/^4He$ ratios

to tag the mantle origin of helium emerging in groundwaters, as discussed earlier in connection with assumption 2, may also hint at a rather broadscale process of volatile supply to the crust. The helium is thought to enter partial melts, including H_2O and CO_2, in the upper mantle, which are emplaced into or plated onto the lower crust. These hot fluids may induce further crustal melting, placing magma bodies into the middle to shallow crust. High $^3He/^4He$ ratios in groundwaters generally correlate with signs of such magmatism (e.g., Welhan et al., 1988), and perhaps because of that there is a certain tendency to assume that the underlying mantle supply of volatiles to the crust is limited to areas of active extensional tectonics. Instead, however, the process may be a more general one, with the extensional areas distinguished only by being regions with horizontal minimum principal stress direction, making it relatively easy for pressurized fluids to make their way upward in the crust. Crustal regions that are active in convergence may have rather similar mantle-fed fluid supply processes at their base, but (as Bailey, 1990, suggests) the fluids are then more readily trapped in horizontal reservoirs at the base of the brittle crust owing to the least principal stress being vertical, and do not lead to abundant surface geochemical emanations. The same argument may be made for a strike-slip regime with some convergence, like the SAF, where the last principal stress in the nearby crust is vertical.

A plausible driving process for the crustal faulting along the San Andreas system is that the crust is coupled, possibly by a weak horizon involving viscous flow in the hot lower crust or along a horizontal detachment, to a mechanically stronger upper mantle. That mantle region is undergoing a shear flow, essentially at steady rate on the interseismic time scale, which results from the Pacific/North America relative plate motion. Such a driving mechanism has been adopted in modeling stress accumulation in earthquake cycles by Li and Rice (1987) and has been discussed recently in terms of rheology and heat flow by Molnar (this volume, Chapter 18). The presumably broadscale shear flow in the upper mantle will result in a modest temperature elevation there, which Molnar (this volume, Chapter 18) suggests as the basis of the broad region of relatively high surface heat flows which encompasses the SAF. Partial melting process should be more active in this slightly warmer shear-flowing region than in adjacent upper mantle, and it should therefore be more effective in supplying volatiles to the base of the overlying crust. Thus there may be an inherent coupling between the flow processes in the upper mantle, which require faulting of the overlying cold crust, and the generation of fluid pressures, which allow that faulting to take place at low stresses.

Water-releasing metamorphic reactions initiated by shear heating of low-grade crustal rocks, as discussed by Scholz (1989, 1990), are also a possible source for highly pressurized fluids within a fault zone. This may be plausible along the SAF in terms of the mineralogy of the Franciscan accretionary complex forming the NE side of the SAF, NW of its intersection with the Garlock fault. Also, the development of deep fluids at high pore pressure along a fault by tectonic compression of adjacent, highly impermeable, fluid-bearing sedimentary rocks has been discussed by Berry (1973) and Irwin and Barnes (1975). Berry (1973) shows many examples of pore pressures well above hydrostatic, and sometimes approaching lithostatic, from borehole records in drilling for oil and gas in the Franciscan complex.

3.3. Assumption 3

The assumption that permeability k is a strongly decreasing function of effective normal stress, and hence a strongly increasing function of pore pressure, has support from

laboratory studies as reported by Brace et al. (1968), Pratt et al. (1977), Brace (1978, 1980), and Huenges and Will (1989). Brace et al. (1968) find that k for intact, unfaulted Westerly granite is decreased from a few hundreds of nanodarcies to a few tens of nanodarcies as the effective confining pressure increases from 0 to 500 bar. Huenges and Will (1989) show that rocks of a given mineralogy with a low value of the bulk modulus at zero confining pressure show a much greater sensitivity of k to effective stress than do rocks of higher bulk modulus. Of course, low bulk modulus denotes a high density of open cracks. This suggests that to the extent that rocks of the heavily deformed fault core are extensively cracked, as suggested in the discussion of assumption 2, they will comply well with assumption 3 and show strong dependence of k on effective stress. Unfortunately, data defining the dependence of k on total stresses $\sigma_{\alpha\beta}$, p, rock type and fabric, and on permeation and temperature history are not as extensive as would be desirable.

We shall assume for the purpose of the simple analysis in the next section that k in the fault is a function only of the effective normal stress $\bar{\sigma} = \sigma - p$, where the total normal stress σ will be assumed to vary linearly with depth over the seismogenic range. Further, some specific results will be shown for the law $k = k_0 \exp(-\bar{\sigma}/\sigma^*)$, where k_0 is the permeability at zero effective stress and where σ^* is a constant. This form provides a tolerable, if very approximate, fit to the experimental results cited above for variations of $\bar{\sigma}$ between 0 and, say, 200–400 bar, when we take $\sigma^* = 50$–400 bar. The lower σ^* values (higher sensitivity to $\bar{\sigma}$) correlate with higher k_0, since they correspond with more highly cracked rocks as noted above.

Thus, for a given σ, k will be a strongly (approximately exponentially) increasing function of p. In the actual situation in a fault zone, where permeability is thought to result from a competition between depositional sealing and rupturing to renew pore connectivity, the strong increase of k with p that we assume here may be interpreted as an approximate proxy for saying that permeability will be negligible unless p is driven up toward σ (e.g., Fyfe et al., 1978). To accommodate such a phenomenon in a simple way, we may use the exponential relation for k just described, but with a yet smaller σ^* (now denoting the range of effective stress over which there is a transition from sealed, or rapidly resealed, to continuously permeable response).

4. Fault Zone and Crustal Pore Pressure Distributions

For simplicity, we model a vertical fault zone through the brittle seismogenic portion of the crust (of thickness $H \approx 15$ km) as a channel of uniform width w (Figure 5), small compared to H, and we start with an extreme form of assumption 2, to be relaxed later. That extreme form considers the adjacent crust to be so impermeable compared to the fault that the ratio $k_{\text{crust}}/k_{\text{fault}} \approx 0$, or, in the alternate/supplementary version of assumption 2, that $k_x/k_z \approx 0$.

For the extreme model described, we take the flow interval within the fault zone to extend vertically from $z = -H$ to the earth's surface at $z = 0$, ignoring the generally complex and permeable aquifer regime at shallow depths. Since there is negligible fluid loss from the fault zone to the crust over that flow interval, the mass rate of fluid upflow in the steady permeation state considered must be the same at every level z. Thus, ignoring variations in fluid mass density, the average (called q here) across the fault channel of the upward volumetric flow rate, q_z, must be independent of z. Letting k be

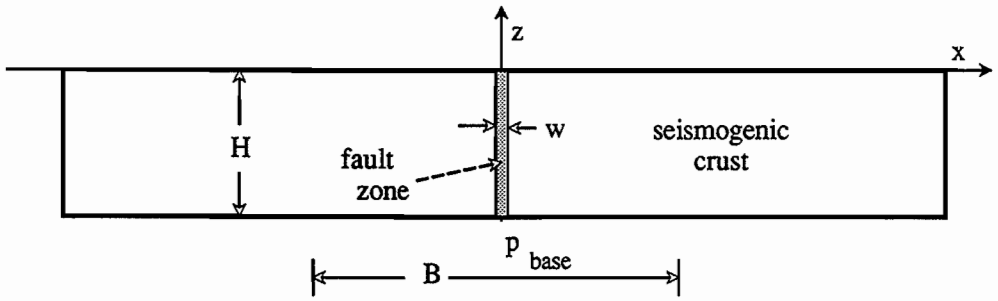

Figure 5. Cross-section of the seismogenic crust; B denotes the width over which elevated pressures are assumed to be present.

the average permeability at level z, letting γ_f be the weight density of the fluid, and noting that in the circumstances described p will be essentially independent of x within the channel, we must therefore have

$$q = -\frac{k}{\eta}\left(\frac{dp}{dz} + \gamma_f\right) = \text{constant (independent of } z)$$

(η is the viscosity of the permeating fluid, taken as constant here). This is to be solved subject to $p = 0$ at $z = 0$, and $p =$ a prescribed pressure, say, p_{base}, at $z = -H$. We will give k a chance to vary with z, as described shortly, but it is interesting to note now that if k is independent of z, then the solution is $p = -p_{\text{base}} z/H$. Thus, if normal stress σ on the fault varies linearly with depth, then the ratio p/σ is independent of depth. This shows that if p is a large fraction of σ at the base of the seismogenic zone, as in assumption 1, then according to this simple solution, p is the same large fraction of σ at every depth.

Now let k vary with z, but according to a law of the type $k = F(\bar{\sigma})$, where $F(\ )$ denotes a function which diminishes very rapidly with increasing values of its argument (shortly, we use the specific form $F(\bar{\sigma}) = k_0 \exp(-\bar{\sigma}/\sigma^*)$ discussed above). Let us write that $\sigma = -(\gamma + \gamma_f)z$ for the variation of σ with z, where γ is constant. If σ is approximately equal to the overburden, then $\gamma = \gamma_t - \gamma_f$ where γ_t is the total weight density of the fault zone material. For numerical illustrations we use $\gamma_f = 0.1$ bar m^{-1} ($= 10^4$ Pa m^{-1}) and $\gamma = 0.2$ bar m^{-1}, and also $H = 15$ km.

Thus, writing $p = \sigma - \bar{\sigma}$, we can rewrite the above equation for the flow rate as

$$\eta q = F(\bar{\sigma})\left(\frac{d\bar{\sigma}}{dz} + \gamma\right)$$

and this may be rearranged to

$$\gamma d(-z) = \frac{d\bar{\sigma}}{1 - \eta q/\gamma F(\bar{\sigma})}$$

Consider what happens as we integrate this equation from the surface, where $z = 0$ and $\bar{\sigma} = 0$, to deeper locations along the fault zone. In this integration, $d(-z) > 0$ and, for solutions of interest, one must conclude that the integration begins with $d\bar{\sigma} > 0$, which means that the (unknown) upflow $q < \gamma F(0)/\eta$ (the right side equals the flow rate due to a hydraulic gradient that is about twice in excess of hydrostatic in a solid with permeability equal to that of unstressed fault material). However, if $F(\bar{\sigma})$ diminishes to

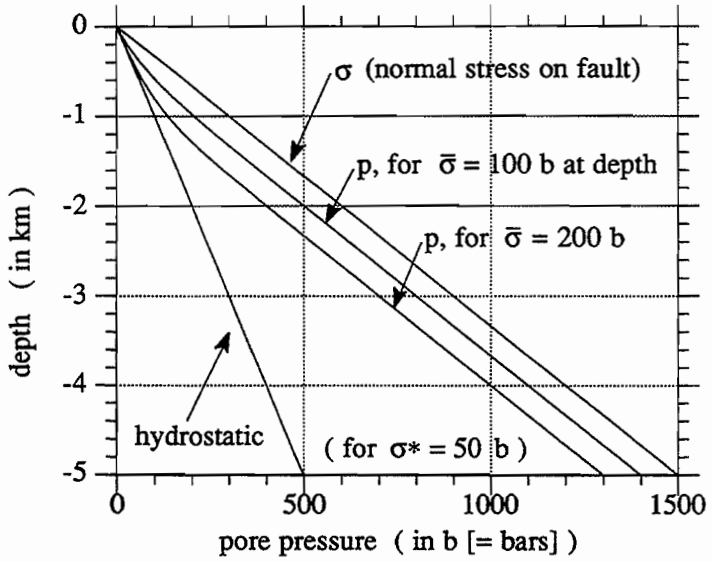

Figure 6. Pore pressure versus depth in fault zone for first 5 km of 15 km seismogenic thickness. The pore pressure distribution adjusts so that the effective normal stress, and thus also the permeability, becomes independent of depth. Based on permeability $k = k_0 \exp(-\bar{\sigma}/\sigma^*)$.

arbitrarily small values with increase of $\bar{\sigma}$, then the denominator in the integration will approach to a zero point as $\bar{\sigma}$ increases, and as that happens the ratio $d\bar{\sigma}/d(-z)$ must approach zero.

Thus the solution for $\bar{\sigma}$ approaches a constant value with increase of depth, that constant value being the solution of $\gamma F(\bar{\sigma}) = \eta q$; see Figure 6. Hence the permeability $k\ [= F(\bar{\sigma})]$ likewise approaches a constant (which legitimizes the assumption made in the simpler analysis above that k could be independent of depth). Thus, assuming that $\bar{\sigma}$ has effectively approached this constant asymptotic value (call that value $\bar{\sigma}_a$, which solves $\gamma F(\bar{\sigma}_a) = \eta q$) before the depth H is reached, the pressure toward the base of the brittle layer will be $p_{\text{base}} = (\gamma + \gamma_f)H - \bar{\sigma}_a$. That pressure is in excess of hydrostatic by the difference $\gamma H - \bar{\sigma}_a$, where γH is of order 3000 bar.

The upflow rate in the fault zone is given by

$$q = \gamma F[\bar{\sigma}_a]/\eta = \gamma F[(\gamma + \gamma_f)H - p_{\text{base}}]/\eta$$
$$\approx 6 \times 10^{14}/\text{year-m} \cdot F(4500 \text{ bar} - p_{\text{base}})$$

with $\eta = 10^{-3}$ Pa s. Thus, if p_{base} is hydrostatic, $p_{\text{base}} \approx 1500$ bar, the permeability function F will be reduced to a size that effectively prohibits flow. While the specifics of a supply mechanism for fluids at the base have not been described here, we might reasonably assume that if there is no venting flow q then p_{base} would not remain hydrostatic. Indeed, it is reasonable to assume that p_{base} increases until a steady state is reached, at which the venting up the fault zone at rate q just balances the supply rate. To have a nonnegligible flow rate, p_{base} will have to be driven upward in magnitude to within a small margin, perhaps within 50–300 bar, of the 4500 bar normal stress at the base.

For the simple exponential approximation $k = F(\bar{\sigma}) = k_0 \exp(-\bar{\sigma}/\sigma^*)$ described earlier, the integration discussed above may be carried out explicitly to give effective

normal stress $\bar{\sigma}$ versus depth in the form

$$\bar{\sigma} = \sigma^* \ln\left(\frac{1}{\alpha + (1-\alpha)\exp(\gamma z/\sigma^*)}\right)$$

where $\alpha = q\eta/\gamma k_0$. This is seen to become asymptotic (as $\gamma z/\sigma^*$ becomes large negative) to the value $\bar{\sigma}_a = \sigma^* \ln(\gamma k_0/\eta q)$, and this value is effectively reached at a depth of about $2\sigma^*/\gamma$, which has the range 150 m to 1.5 km for $\sigma^* = 30$–300 bar. Further, the relation between base pressure and upflow rate is

$$q = \frac{\gamma k_0}{\eta}\exp\left(\frac{-\gamma H}{\sigma^*}\right)\left[\frac{\exp[(p_{\text{base}} - \gamma_f H)/\sigma^*] - 1}{1 - \exp(-\gamma H/\sigma^*)}\right]$$

and since $\gamma H/\sigma^* \approx 10$–$100$ for $\sigma^* = 30$–300 bar, this reduces, whenever p_{base} is at least a little in excess of hydrostatic, to

$$q = \frac{\gamma k_0}{\eta}\exp\left(-\frac{\sigma_{\text{base}} - p_{\text{base}}}{\sigma^*}\right)$$

Figure 6 shows plots of pore pressure p versus depth over the first 5 km for this solution, based on $\sigma^* = 50$ bar. Results are shown for two cases in which the base pressure is such as to make the deep, asymptotically approached, effective normal stress $\bar{\sigma}_a$ equal, respectively, to 100 bar and 200 bar. As seen, the pore pressure rapidly approaches a distribution in which it varies with depth just as does the normal stress σ, but with p reduced by a constant amount ($= \bar{\sigma}_a$) from σ. Similar patterns have sometimes been seen in pressure logs from drilling for oil and gas in the Franciscan adjacent to the SAF, notably at Fort Bragg (Berry, 1973). In another context, Robin (1990) has also recently analyzed permeation with k dependent on effective stress.

Figure 7 shows the volumetric outflow rate per unit area within the fault channel, in millimeters of fluid discharged per year, in terms of the excess of p_{base} over hydrostatic at the bottom of the layer. Results are shown for values of σ^* ranging from 25 to 200 bar, and the curves have been drawn for $k_0 = 1$ md (and taking $\eta = 10^{-3}$ Pa s). In view of the earlier discussion, that relatively high k_0 value might be thought sensible only for the smaller σ^* values shown. It is easy to correct for other cases since the vertical axis in the plot is q times 1 md/k_0. Thus, if $k_0 = 1$ μd is taken as more suitable for the higher σ^* values shown, then the outflow rates plotted are reduced by 10^{-3}.

The response shown by this analysis, for the smaller σ^* values that are preferred for the reasons discussed earlier, reveals a substantial nonlinearity. The venting rate q is negligibly small unless p_{base} rises to become close in value to the lithostatic pressure at the base, and the venting increases very rapidly with p_{base} as that limit is approached, so that the system may be assumed to settle into an equilibrium at which venting balances deeper supply with p_{base} near to its limiting value.

This simple model suggests that the effective normal stress $\bar{\sigma}$ could be essentially independent of depth, within the seismogenic range of a fault zone above a highly pressurized root. This, in turn, implies that the limiting frictional strength, $\tau = f\bar{\sigma}$, may not have much variation with depth. Thus well-known plots of strength versus depth (Brace and Kohlstedt, 1980; Sibson, 1982; etc.), which are governed by brittle friction strength increasing linearly with depth at shallow depth and by ductile flow strength decreasing with depth as depth (and temperature) increase, may require some minor modifications in this case. A pore pressure distribution of the type shown here would deepen, compared to previous estimates, the depth at which frictional strength equals

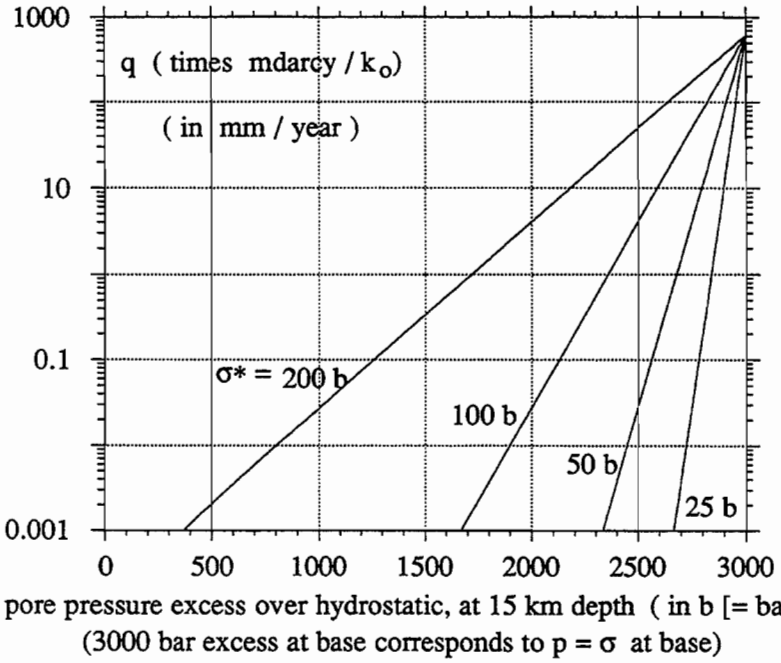

Figure 7. Relation between the fluid upflow rate (q) in the fault zone and the excess of actual pore pressure over hydrostatic at 15 km base of seismogenic zone. Curves drawn for 1 md zero-stress permeability, but can be adjusted to other values as indicated.

creep strength. (In fact, the actual depth of earthquake nucleation may more properly relate to the depth (and temperature) at which friction changes from the potentially unstable velocity-weakening type to the more inherently stable velocity-strengthening type. The relevance of that transition has been shown in earthquake cycle modeling based on rate- and state-dependent friction by Tse and Rice (1986), and foreshadowed by discussions of temperature effects on stick–slip by Brace and Byerlee (1970) and Brace (1972).)

These results show how the assumptions 1 to 3 (with an extreme version of 2) lead to a pore pressure distribution which is high, and near to the fault-normal compression, everywhere throughout the seismogenic zone. That suffices for absolute fault weakness. It remains to be seen that p will be somewhat reduced at points laterally away from the fault zone, in the adjacent crust, as required to explain relative weakness.

In fact, p can be defined in the adjacent crust, on the basis of the analyses just performed, once we specify a distribution of k there (which must be far smaller than k is for the fault, at least throughout the seismogenic layer, for validity of the analysis just described). The result depends on that k distribution and on boundary conditions along the base of layer considered in Figure 5. Rather than dealing with that limiting case directly, we shall consider two types of models where k_c ($= k_{\text{crust}}$) is far lower than k_f ($= k_{\text{fault}}$) but with k_c/k_f nonzero. In these cases the equation determining p is

$$\nabla\cdot[(k/\eta)\nabla(p+\gamma_f z)] = 0$$

where the excess (over hydrostatic) pressure, $p + \gamma_f z$, vanishes at the earth's surface, $z = 0$. At $z = -H$, we set $p + \gamma_f z = p_{\text{base}} - \gamma_f H$ over the interval $-B/2 < x < B/2$, so that B is the width of the pressurized zone (Figure 5). For $|x| > B/2$, we assume that

$p + \gamma_f z = 0$ (i.e., p is hydrostatic there, at $p = \gamma_f H$). Also, to simplify matters, we neglect any explicit dependence of k on p, adjusting very approximately for this by making k_f uniform in depth throughout the fault channel $-w/2 < x < w/2$, and also we continue to take η as constant.

In the first type of model considered, we take k_c to be uniform. This is probably very unrealistic, but will provide a contrast with the second type of model which, effectively, seals-off the lower crust, away from the fault zone, by having k_c decrease with depth to very small values compared to k_f.

For the first type of model (k_c = constant), the pressure distribution in the crust depends strongly on B. For $B \gg H$, the solution in the vicinity of the fault is simply $p = -p_{\text{base}} z/H$ and shows no attenuation of the elevated pressure with distance x from the fault. However, for B of the same order as H, the level contours of excess pore pressure depress significantly as one moves away from the fault zone, especially at typical earthquake nucleation depths (of order 10 km, or about $\frac{2}{3}H$) along the SAF, for cases considered here with $k_c \ll k_f$. Note that a difference of excess pressure between two points at the same depth is the same as the difference in total pore pressure between those points. Figure 8 shows such results (the view is of the half of the seismogenic layer, in the region $x > 0$ only) in the case for which $B = 1.52H$ and $k_c = 10^{-2} k_f$, with fault zone width $w = 0.05H$. The contour lines are equally spaced and the change in excess pore pressure from line to line corresponds to 1/10 of the excess pore pressure at the base. These were calculated on the basis of the analogy between steady heat conduction and steady fluid permeation, using the finite-element program ABAQUS to solve for the temperature field in an analogously inhomogeneous medium. If the excess pressure is of order 3000 bar at the base, then the contour spacing is of order 300 bars excess pressure.

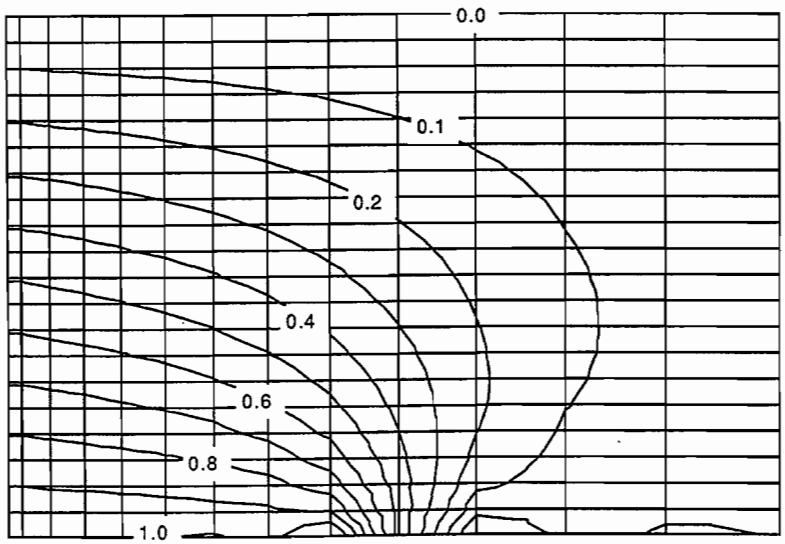

Figure 8. Contours of constant excess pore pressure, $p + \gamma_f z$, for the region of Figure 5 with $x > 0$, when the crustal permeability is uniform at 1/100 of the fault zone permeability. Calculation done for fault width $w = 0.05H$ and pressurized base width $B = 1.52H$. Numbers on contours give local value of excess pore pressure as a fraction of $p_{\text{base}} - \gamma_f H$. Contour spacing of 1/10 of the excess pore pressure at the base corresponds to a contour interval of about 300 bar when the base pressure is lithostatic.

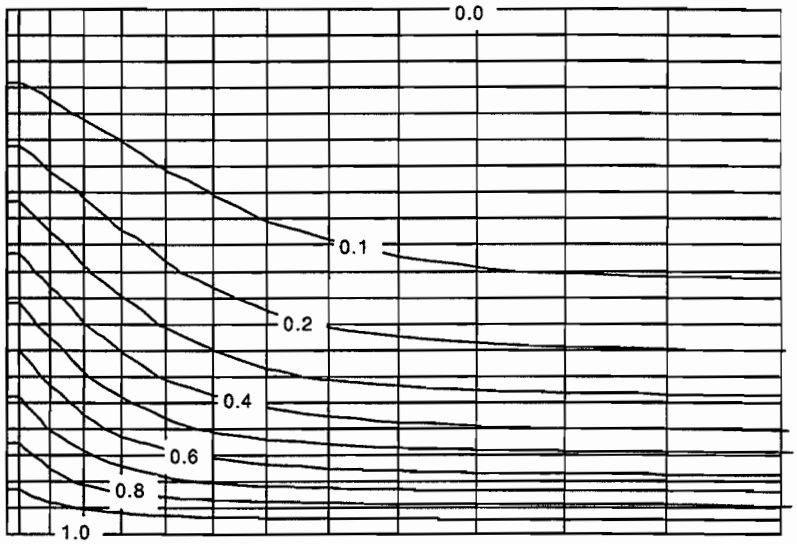

Figure 9. Contours of constant excess pore pressure, $p + \gamma_f z$, for the region of Figure 5 with $x > 0$, when the crustal permeability decreases exponentially with depth, from 1/10 of the fault zone permeability at the surface to 1/1000 of the fault zone permeability at the base. Calculation done for fault width $w = 0.05H$ and pressurized base width B extending over full width. Numbers on contours give local value of excess pore pressure as a fraction of $p_{\text{base}} - \gamma_f H$. Contour spacing of 1/10 of the excess pore pressure at the base corresponds to a contour interval of about 300 bar when the base pressure is lithostatic.

The second type of model examined significantly decreases the crustal permeability with depth. Now the results are insensitive to B, which can be taken as large as the overall width considered. Figure 9 shows results, again from ABAQUS via the steady heat conduction analogy, when the crustal permeability decreases with depth according to the relation $k_c = k_f 10^{-1+2z/H}$, so that $k_c = 10^{-1} k_f$ at the surface, $z = 0$, but k_c diminishes to $10^{-3} k_f$ at the base of the seismogenic layer, $z = -H$. The contours of excess pressure have the same spacing as above, and these are again seen to show higher p in the fault zone than at a small distance away, at the same depth, in the adjacent crust. Although the permeability of the middle depth range of the seismogenic crust is about the same here as in the previous example, the effect of distributing the low permeability toward the lower part of the seismogenic zone has a major effect on attenuating the excess pressure at points laterally away from the fault zone.

An alternative, or supplementary, version of assumption 2 was stated, for which horizontal permeability in the fault zone is far less than vertical. It is evident that such a property distribution will also attenuate the excess pore pressure at points laterally away from the fault zone.

At this point we may conclude that assumptions 1 to 3 lead to pore pressure distributions in the fault zone and in the nearby crust which are of the type noted earlier to be consistent with both the absolute and relative weakness of the SAF.

5. Vertically Propagating Pressure Pulses

For a simple analysis of time-dependent processes associated with the strongly nonlinear dependence of k on effective stress, we may return to the extreme form of assumption 2

adopted in the last section, in which mass outflow from the fault channel into the, presumably, much less permeable crust is neglected. Thus, if $m = m(z, t)$ is the average across the fault channel, at vertical position z, of the mass of fluid contained in unit volume of fault zone material, mass conservation requires that

$$\frac{\partial q}{\partial z} + \frac{\partial m}{\partial t} = 0$$

Although more accurate porous medium theories are possible, it is simplest to assume that m is a function only of the effective stress $\bar{\sigma} = \sigma - p$, that is, $m = G(\bar{\sigma})$. Thus with $k = F(\bar{\sigma})$ as before, we have

$$\frac{\partial}{\partial z}\left[-\frac{\rho_f}{\eta} F(\sigma - p)\left(\frac{\partial p}{\partial z} + \gamma_f\right)\right] + \frac{\partial}{\partial t}[G(\sigma - p)] = 0$$

for the equation controlling time dependence of pore pressure, where ρ_f is the mass density of fluid, regarded as constant here. Again, the normal stress σ is assumed in the form $\sigma = -(\gamma + \gamma_f)z$ as earlier, so that the previous equation can be rewritten as

$$\frac{\partial}{\partial z}\left[\frac{\rho_f}{\eta} F(\bar{\sigma})\left(\frac{\partial \bar{\sigma}}{\partial z} + \gamma\right)\right] + \frac{\partial}{\partial t}[G(\bar{\sigma})] = 0$$

If the fluids in the fault zone are mainly in cracklike pore spaces, as may be reasonable for a high pore pressure situation, it is reasonable to expect that k varies approximately with the cube of openings between the cracklike cavity walls (Poiseuille flow), but that m varies approximately with only the first power of those openings. In that case, and perhaps in others, it is reasonable to expect that $F(\bar{\sigma})$, which gives k, will be a much more rapidly varying function of $\bar{\sigma}$ than is $G(\bar{\sigma})$, which gives m. Formally, we may express this as saying that $F(\bar{\sigma})$ and $G(\bar{\sigma})$, both of which are assumed to decrease monotonically with increasing $\bar{\sigma}$, are also assumed to satisfy the inequality

$$\frac{F(\bar{\sigma}) - F(\bar{\sigma}_2)}{F(\bar{\sigma}_1) - F(\bar{\sigma}_2)} < \frac{G(\bar{\sigma}) - G(\bar{\sigma}_2)}{G(\bar{\sigma}_1) - G(\bar{\sigma}_2)} \qquad \text{for } \bar{\sigma}_1 < \bar{\sigma} < \bar{\sigma}_2$$

To make this inequality a little less abstract, suppose that F is proportional to h^3 and G to h, where h is some representative open width of cracklike, fluid-filled cavities in the fault zone, and h decreases with increasing $\bar{\sigma}$ so that $h_1 > h_2$ if $\bar{\sigma}_1 < \bar{\sigma}_2$. Then the above inequality is equivalent to the self-evident inequality

$$\frac{h^3 - h_2^3}{h_1^3 - h_2^3} \equiv \frac{(h - h_2)(h^2 + hh_2 + h_2^2)}{(h_1 - h_2)(h_1^2 + h_1 h_2 + h_2^2)} < \frac{(h - h_2)}{(h_1 - h_2)} \qquad \text{for } h_1 > h > h_2$$

The above inequality in F and G is important, because it is the feature which suffices to give wavelike solutions for the upward propagation of a surge in pore pressure (decrease in $\bar{\sigma}$) due to an increase of pore pressure deep in the fault zone. Such deep increase might result from the shear rupture of a low-permeability barrier which has trapped fluid at more highly elevated pressures below.

Let us suppose then that the pore pressure distribution is initially in an asymptotic steady state with $\bar{\sigma}$ $(= \sigma - p)$ constant with respect to depth and $\partial p/\partial z = d\sigma/dz = -(\gamma + \gamma_f)$, as discussed earlier and shown in Figure 6. Let $\bar{\sigma}_0$ be that initial $\bar{\sigma}$ value. We seek to see when a solitary wave solution of form $\bar{\sigma}$ = function of $z - Vt$ could exist, which takes $\bar{\sigma}$ from its initial value $\bar{\sigma}_0$ to a final value $\bar{\sigma}_f$, as the

wave passes by, and also to find the speed V of the wave. For such a wave field we can replace $\partial/\partial t$ by $-V\partial/\partial z$ in the above partial differential equation and then integrate it in z, from a position well ahead of the wavefront, where $\bar{\sigma} = \bar{\sigma}_0$, to one at a general state $\bar{\sigma}$ within the variable part of the wave, to one behind the wavefront where the new state $\bar{\sigma} = \bar{\sigma}_f$ has been established. Thus, fixing attention on any convenient moment of time and, to focus on the variation of $\bar{\sigma}$ with z, replacing $\partial\bar{\sigma}/\partial z$ with $\mathrm{d}\bar{\sigma}/dz$, we have

$$\rho_f F(\bar{\sigma})\left(\frac{d\bar{\sigma}}{dz} + \gamma\right) - \eta V G(\bar{\sigma}) = \rho_f \gamma F(\bar{\sigma}_0) - \eta V G(\bar{\sigma}_0) = \rho_f \gamma F(\bar{\sigma}_f) - \eta V G(\bar{\sigma}_f)$$

Thus, if such a wave exists, the last equality of this expression shows that its velocity will be

$$V = \frac{\rho_f \gamma}{\eta} \frac{F(\bar{\sigma}_f) - F(\bar{\sigma}_0)}{G(\bar{\sigma}_f) - G(\bar{\sigma}_0)}$$

The monotonicity of F and G shows that this expression for V always yields a positive result. Hence, if such wavelike propagation of a pore pressure change can occur at all, it must involve an upwardly propagating pulse.

To see whether the wave can occur we substitute the expression for V into the expression before it, and then solve for $d\bar{\sigma}/dz$ to obtain

$$\frac{d\bar{\sigma}}{dz} = \frac{\gamma[F(\bar{\sigma}_f) - F(\bar{\sigma}_0)]}{F(\bar{\sigma})}\left[\frac{G(\bar{\sigma}) - G(\bar{\sigma}_0)}{G(\bar{\sigma}_f) - G(\bar{\sigma}_0)} - \frac{F(\bar{\sigma}) - F(\bar{\sigma}_0)}{F(\bar{\sigma}_f) - F(\bar{\sigma}_0)}\right]$$

By integrating in the positive direction in z, from the state of $\bar{\sigma} = \bar{\sigma}_f$ to that at $\bar{\sigma} = \bar{\sigma}_0$ (the corresponding z values in this type of wave analysis are at $-\infty$ and $+\infty$), this equation defines the variation in $\bar{\sigma}$ across the wavefront. A consistent result is obtained if z increases in the positive direction as $\bar{\sigma}$ is varied from $\bar{\sigma}_f$ to $\bar{\sigma}_0$, and such a result ($dz > 0$) is assured if the right-hand side of this equation is of the same sign as $\bar{\sigma}_0 - \bar{\sigma}_f$ when $\bar{\sigma}$ lies between $\bar{\sigma}_f$ and $\bar{\sigma}_0$. Because of the monotonic decrease of F with $\bar{\sigma}$, $[F(\bar{\sigma}_f) - F(\bar{\sigma}_0)]$ is always of that sign. The inequality involving F and G assumed earlier then assures us that the long bracketed set of terms on the right side of this equation also have the same sign as $\bar{\sigma}_0 - \bar{\sigma}_f$, at least when $\bar{\sigma}$ lies between $\bar{\sigma}_f$ and $\bar{\sigma}_0$. Thus the right-hand side is always positive when $\bar{\sigma}$ lies between $\bar{\sigma}_f$ and $\bar{\sigma}_0$, which therefore tells us that a wavelike solution can exist only when $\bar{\sigma}_0 - \bar{\sigma}_f > 0$.

Hence a wavelike solution exists only when it is a state with smaller $\bar{\sigma}$, or higher pore pressure, that is being propagated upward into the initial state. This will correspond to an upward surge of pore fluid.

The expression above for the velocity V of the surge reduces to a simple form when the decrease in $\bar{\sigma}$ is sufficiently strong that we may assume that $F(\bar{\sigma}_0)$ and $G(\bar{\sigma}_0)$ are, respectively, small compared to $F(\bar{\sigma}_f)$ and $G(\bar{\sigma}_f)$. In that limit the speed is

$$V = \frac{\rho_f \gamma k}{\eta m} = \frac{\gamma k}{\eta n}$$

where the k and m are those in the state behind the wavefront (that with $\bar{\sigma}$ denoted as $\bar{\sigma}_f$ above), and the latter form of the result arises when we write $m = \rho_f n$, where n is the fluid-filled porosity in the fault zone. Not unexpectedly, that latter term may be recognized as the average fluid particle velocity in a porous medium under an excess pressure gradient of γ.

To examine representative numerical values, if we assume $k = 1$ md, γ and η as before,

and assume a porosity of $n = 0.01$, this gives $V = 60$ m/year. Values on the order of 1 km/year at not implausible for strong pressure surges which initiate additional microcracking, and result in a large increase in permeability to the 10–100 md range (they would, presumably, also involve a somewhat larger n). There may be a connection between the upwardly propagating surges, shown to result from the analysis here, and the unstably rising 'fluid domains' hypothesized by Gold and Soter (1985).

This analysis of pressure surges is an incomplete treatment of time effects, not only because it examines only a particular type of solution to the partial differential equation, but because it does not include explicit treatment of dissolution and deposition which, in aggregate, are thought to seal off permeability (Smith and Evans, 1984; Nur and Walder, 1990), and of shear rupturing processes which can renew pore connectivity and hence restore permeability. Time-dependent pore pressure has been emphasized by Gold and Soter (1985) and Sibson (1990) as a factor in addition to tectonic loading which could control the timing and aperiodicity of earthquakes.

6. Summary

It has been shown that a pore pressure distribution with p high and near to the fault-normal compression in a major fault zone such as the SAF, but somewhat lower in the adjacent crust, is consistent with the absolute and relative weakness of that major fault. This result remains valid for friction coefficients f in the typical range of 0.6–0.9 as for laboratory data on crustal rocks. Previously, such a pore pressure explanation has been regarded as invalid, since pore pressures within the fault zone would have to exceed the overburden there. However, it is shown here that a maturely deformed fault zone, weakened either by high pore pressure or by inherently weak material, will develop a stress state within its active core which is different from the state in the nearby crust. In particular, for the situation of a vertical strike-slip fault that is driven by stresses in the adjoining crust which have a maximum principal direction at a steep angle to the fault trace (and which are suitable for inducing thrust failures in the crust), all principal stress values in the active strike-slip fault core are elevated over those at the same depth in the adjoining crust. Because of that feature, high pore pressure distributions, as described, are possible with p less than the least principal stress at every point of the medium, even though p in the fault core may exceed the least principal stress σ_3 at some distance away in the crust (where, typically, adjacent to the SAF, σ_3 equals the overburden).

Three assumptions concerning the presence and motion of fluids in the crust were introduced. It was shown that these assumptions, when implemented as the basis for a steady-state fluid permeation analysis, lead to the type of pore pressure distributions which have been noted above to be consistent with both absolute and relative fault weakness. Briefly, the assumptions are that pore fluids are present near the ductile roots of fault zones, that active fault zones maintain a far higher permeability than do adjacent regions of the crust, and that permeability in the fault zone is a strongly decreasing function of the effective normal stress. This set of assumptions has support from a variety of sources, discussed in this chapter. These include laboratory rock permeability measurements, petrologic studies of exhumed fault zone rocks, geochemical characterization of groundwater outflows near faults, magnetotelluric inferences of electrical conductivity

in the middle and lower crust, and seismic studies of wave speed and attenuation variations near active faults.

While the results of this chapter do not invalidate other possible explanations of weakness along major faults such as the SAF, they do show that elevated pore pressure is a plausible explanation. Deep drilling to the near vicinity of an active major fault zone, with measurement of stress state and pore pressure variations as the fault zone is approached, could provide a critical test of these ideas. If the pore pressure explanation of fault weakness is correct, then the traditional concept of frictional strength in the brittle crust varying in an approximately linear manner with depth must be replaced by one in which frictional strength is relatively uniform with respect to depth throughout the seismogenic zone.

Additional features of interest for earthquake phenomena follow from the assumptions made in the fluid permeation analysis. For example, it is shown that the time-dependent equations for the effective stress and pore pressure distributions without the fault zone have wavelike solutions corresponding to surges of pore pressure, and of pore fluid, which slowly make their way upward in a fault zone. Also, while the concept is not developed here, pore pressure distributions that result from a nonlinear, effective stress-dependent permeability provide new insights on the possible origins of seismic asperities. In addition to being due to variations in inherent frictional properties within the fault zone, such asperities may also result from variations in permeability properties (e.g., in properties analogous to k_0 and σ^* in the simple exponential model introduced here), or from fluctuations about the approximately linear variation of normal stress with depth.

It is a delight to dedicate this chapter to William F. Brace, whose work over many years has contributed richly to many of the areas discussed. The work was presented orally in June 1990 at a conference in honor of Brace.

Acknowledgment

Support for this study was provided by the USGS under grant 14-08-0001-G-1788 to Harvard. Also, the program ABAQUS was kindly made available under academic licence by Hibbitt, Karlsson and Sorensen, Inc. of Providence, RI. I am grateful to many individuals for discussing the concepts of this chapter. Robert Newton of Chicago posed some interesting questions to me in late 1988 which began the thinking leading to this work. Helpful discussions, verbally and/or by correspondence, were had also with Atilla Aydin, Fred Chester, Harmon Craig, Jack Hermance, Steve Hickman, William Irwin, Louise Kellogg, Geoff King, John Logan, Ted Madden, Brian Mitchell, Julie Morris, Kieth O'Nions, Alan Rubin, Selvyn Sacks, Chris Scholz, Tom Shankland, Brian Stewart, Terry Tullis, Hiroshi Wakita, Chi-Yuen Wang, Youxue Zhang, and Mark Zoback.

References

Al-Shukri, H.J. and Mitchell, B.J. (1988). Reduced seismic velocities in the source zone of New Madrid earthquakes. *Bull. Seismol. Soc. Am.* **78**, 1491–1509.

Al-Shukri, H.J. and Mitchell, B.J. (1990). Three-dimensional attenuation structure in and around the New Madrid seismic zone. *Bull. Seismol. Soc. Am.* **80**, 615–632.

Arch, J. and Maltman, A. (1990). Anisotropic permeability and tortuosity in deformed wet sediments. *J. Geophys. Res.* **95**, 9035–9045.

Bailey, R.C. (1990). Trapping of aqueous fluids in the deep crust. *Geophys. Res. Lett.* **17**, 1129–1132.

Beach, A. (1980). Retrogressive metamorphic processes in shear zones with special reference to the Lewisian complex. *J. Struct. Geol.* **2**(1/2), 257–263.

Berry, F.A.F. (1973). High fluid potentials in California Coast Ranges and their tectonic significance. *Bull. Assoc. Petrol. Geol.* **57**, 1219–1249.

Brace, W.F. (1978). A note on permeability changes in geologic material due to stress. *Pure Appl. Geophys.* **116**, 627–633.

Brace, W.F. (1972). Laboratory studies of stick-slip and their application to earthquakes. In *Forerunners of Strong Earthquakes* (eds. E.F. Savarensky and T. Rikitake) *Tectonophysics* **14**(3/4), 189–200.

Brace, W.F. (1980). Permeability of crystalline and argillaceous rocks. *Int. J. Rock Mech. Min. Sci.* **17**, 241–251.

Brace, W.F. and Byerlee, J.D. (1970). California earthquakes: why only shallow focus? *Science* **168**, 1573–1575.

Brace, W.F. and Kohlstedt, D.L. (1980). Limits on lithospheric stress imposed by laboratory experiments. *J. Geophys. Res.* **85**, 6248–6252.

Brace, W.F., Walsh, J.B., and Frangos, W.T. (1968). Permeability of granite under high pressure. *J. Geophys. Res.* **73**(6), 2225–2236.

Byerlee, J.D. (1978). Friction of rocks. *Pure Appl. Geophys.* **116**, 615–626.

Byerlee, J.D. (1990). Friction, overpressure and fault normal compression. *Geophys. Res. Lett.* **17**, 2109–2112.

Byrne, T. and Fisher, D. (1990). Evidence for a weak and overpressurized decollement beneath sediment-dominated accretionary prisms. *J. Geophys. Res.* **95**, 9081–9097.

Chen, W.-P. and Molnar, P. (1983). Focal depths of intracontinental and intraplate earthquakes and their implications for the thermal and mechanical properties of the lithosphere. *J. Geophys. Res.* **88**, 4183–4214.

Etheridge, M.A., Wall, V.J., Cox, S.F., and Vernon, R.H. (1984). High fluid pressures during regional metamorphism and deformation: implications for mass transport and deformation mechanisms. *J. Geophys. Res.* **89**, 4344–4358.

Fournier, R.L. (1990). A San Andreas Fault model in which maximum principal stress nearly normal to the fault is advantageous (abstract). *EOS, Trans. AGU* **71**, 1635.

Fyfe, W.S., Price, N.J., and Thompson, A.B. (1978). *Fluids in the Earth's Crust*, Developments in Geochemistry 1. Elsevier Scientific, New York.

Gold, T. and Soter, S. (1985). Fluid ascent through the solid lithosphere and its relation to earthquakes. *Pure Appl. Geophys.* **122**, 492–530.

Gough, D.I. (1986). Seismic reflectors, conductivity, water and stress in the continental crust. *Nature* **323**, 143–144.

Haak, V. and Hutton, R. (1986). Electrical resistivity in continental lower crust. In *The Nature of the Lower Continental Crust* (eds. J.B. Dawson et al.), pp. 35–49. Geological Society of London Special Publication No. 24.

Hamilton, R.M. and Mooney, W.D. (1990). Seismic-wave attenuation associated with crustal faults in the New Madrid seismic zone. *Science* **248**, 351–354.

Hickman, S. (1991). Stress in the lithosphere and the strength of active faults. *Rev. Geophys.*, Supplement, pp. 759–775, April.

Hubbert, M.K. and Rubey, W.W. (1959). Role of fluid pressure in the mechanics of overthrust faulting I: Mechanics of fluid-filled porous solids and its application to overthrust faulting. *Geol. Soc. Am. Bull.* **70**, 115–166.

Huenges, E. and Will, G. (1989). Permeability, bulk modulus and complex resistivity in crystalline rocks. In *Fluid Movements – Element Transport and the Composition of the Deep Crust* (ed. D. Bridgwater), pp. 361–375. Kluwer, Dordrecht.

Hyndman, R.D. and Shearer, P.M. (1989). Water in the lower continental crust: modelling

magnetotelluric and seismic reflection results. *Geophys. J. Int.* **98**, 343–365.
Irwin, W.P. and Barnes, I. (1975). Effects of geologic structure and metamorphic fluids on seismic behavior of the San Andreas fault system in central and northern California. *Geology* **3**, 713–716.
Irwin, W.P. and Barnes, I. (1980). Tectonic relations of carbon dioxide discharges and earthquakes. *J. Geophys. Res.* **85**(B6), 3115–3121.
Jones, L.M. (1988). Focal mechanisms and the state of stress on the San Andreas fault in Southern California. *J. Geophys. Res.* **93**, 8869–8891.
Kerrich, R. (1986). Fluid infiltration into fault zones: chemical isotopic and mechanical effects. *Pure Appl. Geophys.* **124**, 225–268.
Lachenbruch, A.H. and Sass, J.H. (1980). Heat flow and energetics of the San Andreas fault zone. *J. Geophys. Res.* **85**, 6185–6222.
Li, V.C. and Rice, J.R. (1987). Crustal deformation in great California earthquake cycles. *J. Geophys. Res.* **92**, 11533–11551.
Madden, T., La Torraca, G., and Park, S. (1990). Resistivity variations around the Palmdale section of the San Andreas; unpublished manuscript.
McCaig, A.M. (1988). Deep fluid circulation in fault zones. *Geology* **16**, 867–870.
Meissner, R. and Strehlau, J. (1982). Limits of stress in continental crusts and their relation to the depth-frequency distribution of shallow earthquakes. *Tectonics* **1**, 73–89.
Mooney, W.D. and Ginzburg, A. (1986). Seismic measurements of the internal properties of fault zones. *Pure Appl. Geophys.* **124**, 141–157.
Nagao, K., Kita, I., Matsuda, J., and Ercan, T. (1990). Helium and carbon isotopic composition of gas and water samples from Turkey (abstract). *EOS, Trans. AGU* **71**(28), 850–851.
Newton, R.C. (1989). Metamorphic fluids in the deep crust. *Annu. Rev. Earth Planet. Sci.* **17**, 385–412.
Newton, R.C. (1990). Fluids and shear zones in the deep crust. *Tectonophysics* **182**, 21–37. [Issue on *The Nature of the Lower Continental Crust* (eds. D.M. Fountain and A. Boriani.)]
Newton, R.C., Smith, J.V., and Windley, B.F. (1980). Carbonic metamorphism, granulites and crustal growth. *Nature* **288**, 45–50.
Nur, A. and Walder, J. (1990). Time-dependent hydraulics of the earth's crust. In *The Role of Fluids in Crustal Processes*, pp. 113–127. National Academy Press, Washington, D.C.
O'Nions, R.K. and Oxburgh, E.R. (1988). Helium, volatile fluxes and the development of continental crust. *Earth Planet. Sci. Lett.* **90**, 331–347.
O'Nions, R.K., Griesshaber, E., and Oxburgh, E.R. (1989). Rocks that are too hot to handle. *Nature* **341**, 391.
Oppenheimer, D.H., Reasenberg, P.A., and Simpson, R. (1988). Fault plane solutions for the 1984 Morgan Hill earthquake sequence: evidence for the state of stress on the Calaveras fault. *J. Geophys. Res.* **93**, 9007–9026.
Oxburgh, E.R. and O'Nions, R.K. (1987). Helium loss, tectonics, and the terrestrial heat budget. *Science* **237**, 1583–1588.
Parry, W.T. and Bruhn, R.L. (1986). Pore fluid and seismogenic characteristics of fault rock at depth on the Wasatch fault, Utah. *J. Geophys. Res.* **91**, 730–734.
Peacock, S.M. (1990). Fluid processes in subduction zones. *Science* **248**, 329–337.
Pratt, H.R., Black, A.D., Brace, W.F., and Swolfs, H. (1977). Elastic and transport properties of an in-situ jointed granite. *Int. J. Rock Mech. Min. Sci.* **14**, 35–45.
Raleigh, C.B., Healy, J.H., and Bredehoeft, J.D. (1976). An experiment in earthquake control at Rangely, Colorado. *Science* **191**, 1230–1237.
Robin, P.-Y.F. (1990). Water retention within a brittle upper crust: a numerical simulation. Abstract of presentation at Brace Symposium: Fault Mechanics and Transport Properties of Rock, MIT, June 1990.
Scholz, C.H. (1989). Mechanics of faulting. *Annu. Rev. Earth Planet. Sci.* **17**, 309–334.
Scholz, C.H. (1990). *The Mechanics of Earthquakes and Faulting.* Cambridge University Press.
Shankland, T.J. and Ander, M.E. (1983). Electrical conductivity, temperatures, and fluids in the lower crust. *J. Geophys. Res.* **88**, 9475–9484.

Sheppard, S.M.R. (1989). The isotopic characterization of aqueous and leucogranitic crustal fluids. In *Fluid Movements – Element Transport and the Composition of the Deep Crust* (ed. D. Bridgwater), pp. 245–263. Kluwer, Dordrecht.

Sibson, R.H. (1982). Fault zone models, heat flow, and the depth distribution of earthquakes in the continental crust of the United States. *Bull. Seismol. Soc. Am.* **72**, 151–163.

Sibson, R.H. (1985). A note on fault reactivation. *J. Struct. Geol.* **7**, 751–754.

Sibson, R.H. (1990). Rupture nucleation on unfavorably oriented faults. *Bull. Seismol. Soc. Am.* **80**, 1580–1604.

Sibson, R.H., McMoore, J., and Rankine, A.H. (1975). Seismic pumping – A hydrothermal fluid transport mechanism. *J. Geol. Soc. London* **131**, 653–659.

Smith, D.L. and Evans, B. (1984). Diffusional crack healing in quartz. *J. Geophys. Res.* **89**, 4125–4135.

Tse, S.T. and Rice, J.R. (1986). Crustal earthquake instability in relation to the depth variation of frictional slip properties. *J. Geophys. Res.* **91**, 9452–9472.

Wakita, H., Fujii, N., Matsuo, S., Notsu, K., Nagao, K., Takaoka, N. (1978). 'Helium spots': caused by a diapiric magma from the upper mantle. *Science* **200**, 430–432.

Wakita, H., Sano, Y., and Mizoue, M. (1987). High ^{3}He emanation and seismic swarms observed in a nonvolcanic, forearc region. *J. Geophys. Res.* **92**, 12539–12546.

Wang, C.-Y., Rui, F., Zhengsheng, Y., and Xingjue, S. (1986). Gravity anomaly and density structure of the San Andreas fault zone. *Pure Appl. Geophys.* **124**, 127–140.

Welhan, J.A., Poreda, R.J., Rison, W., and Craig, H. (1988). Helium isotopes in geothermal and volcanic gases of the western United States, I. Regional variability and magmatic origin. *J. Volcanol. Geotherm. Res.* **34**, 185–199.

Wilcock, W.S.D., Purdy, G.M., and Solomon, S.C. (1990). Microearthquake evidence for extension across the Kane transform fault. *J. Geophys. Res.* **95**, 15439–15462.

Zoback, M.D. and Healy, J.H. (1991). In situ stress measurements to 3.5 km depth in the Cajon Pass scientific research borehole: implications for the mechanics of crustal faulting, *J. Geophys. Res.*, in press.

Zoback, M.D., Tsukahara, H., and Hickman, S. (1980). Stress measurements at depth in the vicinity of the San Andreas fault: implications for the magnitude of shear stress at depth. *J. Geophys. Res.* **85**, 6157–6173.

Zoback, M.D., Zoback, M.L., Mount, V.S., Suppe, J., Eaton, J.P., Healy, J.H., Oppenheimer, D., Reasenberg, P., Jones, L., Raleigh, C.B., Wong, I.G., Scotti, O., and Wentworth, C. (1987). New evidence on the state of stress on the San Andreas fault system. *Science* **238**, 1105–1111.